Geophys. J. R. astr. Soc. (1977) **50**, 215–233

Far-field waveforms from an arbitrarily expanding, transparent spherical cavity in a prestressed medium

J. B. Minster and A. M. Suteau *California Institute of Technology, Seismological Laboratory, Pasadena, California 91125, USA*

Received 1976 November 3; in original form 1976 August 23

Summary. Stress relaxation due to a growing cavity in a uniformly prestressed (pure shear) elastic medium is investigated, using the transparent source approximation of Archambeau (1972). A simple representation of the far-field radiation is obtained. A planar, circular dislocation of same growth history as the cavity is constructed which yields the same far-field pulses, except for geometrical effects. It is shown that different 'equivalent' dislocations must be used to model P and S pulses wherever the rupture velocity is trans-sonic. Simple analytical forms for the far-field pulses are derived which hold even in the case of relatively complicated source growth history. The dependence of waveforms on the various source parameters is illustrated by selected waveform calculations. It is suggested that this model yields an adequate representation of the far-field tectonic release radiation from underground explosions.

Introduction

It has long been evident that the detonation of an underground nuclear explosion in a prestressed medium gives rise to an anomalous radiation field, in addition to the compressional waves generated by the explosion itself. This anomalous radiation is mostly visible in the presence of *SH* and Love waves (e.g. Lambert, Flinn & Archambeau 1972), and cannot be distinguished from a double-couple radiation. Interpretations of this anomalous radiation fall in two classes: (1) the induced earthquake theory (e.g. Brune & Pomeroy 1963; Aki 1964; Aki *et al.* 1969) and (2) the stress relaxation theory (e.g. Archambeau & Sammis 1970; Archambeau 1972). As pointed out by Archambeau, the phenomenon always amounts to some form of stress relaxation: in particular, if the medium was prestressed prior to the detonation, there must be an anomalous radiation, whether large-scale faulting occurs or not. In fact, a survey of the literature shows convincing arguments in favour of both cases.

This provides strong motivation for the investigation of the elastodynamic radiation associated with the creation of a cavity in a prestressed medium (e.g. Randall 1964; Archambeau 1964, 1972; Hirasawa & Sato 1963; Koyama, Horiuchi & Hirasawa 1973; Snoke 1976). Most investigations so far have been performed in the spectral domain, although solutions have been obtained in the time domain for simple cases (Burridge 1975; Harkrider 1976).

However, time-domain results are often complicated and rather cumbersome to use. In this paper we investigate the far-field equivalent source, and make a detailed comparison of a relaxation mechanism due to the creation of a cavity, and a dislocation of same growth history and moment. The results are obtained in a simple analytical form, particularly suitable for computation. We investigate not only the use of a constant rupture velocity, but also time-varying rupture velocities which can be successively supersonic, trans-sonic, and subsonic, and illustrate the analytical results with a variety of numerical calculations.

1 Stress relaxation induced by an explosion in a prestressed medium

Snoke (1976) gives a detailed comparison of the far-field radiation due to

(1) The instantaneous creation of a spherical cavity in a prestressed medium.
(2) The application of a pressure pulse on the cavity wall.
(3) The instantaneous creation of a circular dislocation.

In this Section we propose to extend his results to the more general case where failure occurs over a finite time instead of instantaneously.

Details of the theory can be found in Archambeau (1968, 1972) or Minster (1973). The problem is treated as a generalized initial value problem, which is solved using a Green's function technique. The failure zone is assumed to be transparent to incident radiation, which amounts to ignoring the oscillations of the cavity (Minster 1973; Burridge 1975). Because this approximation is used, boundary conditions at the surface of the sphere are ignored and whether we deal with an actual cavity or with a spherical failure zone with no shear resistance does not affect the solution. The far-field displacement radiation spectrum may be written, in spherical coordinates,

$$\left.\begin{aligned} \tilde{u}_r(\mathbf{r}, \omega) &= -\tilde{\psi}_4 \\ \tilde{u}_\theta(\mathbf{r}, \omega) &= 2[\sin\phi\,\tilde{\psi}_1 - \cos\phi\,\tilde{\psi}_2] \\ \tilde{u}_\phi(\mathbf{r}, \omega) &= 2[\cos\theta\cos\phi\,\tilde{\psi}_1 + \cos\theta\sin\phi\,\tilde{\psi}_2 - \sin\theta\,\tilde{\psi}_3] \end{aligned}\right\} \tag{1.1}$$

Here, the quantities $\tilde{\psi}_\alpha$, $\alpha = 1, \ldots, 4$ are given by

$$\tilde{\psi}_\alpha = \frac{1}{k_\alpha^2}\frac{\partial}{\partial r}\tilde{\chi}_\alpha \tag{1.2}$$

where $k_4 = k_p = \omega/V_p$, $k_i = k_s = \omega/V_s$, $i = 1, 2, 3$, and $\tilde{\chi}_4(r, \omega)$ is the dilatation potential, whereas $\tilde{\chi}_i$, $i = 1, 2, 3$ are the Cartesian components of the rotation potential. These potentials can be expressed in the form of general multipolar expansions

$$\tilde{\chi}_\alpha(r, \omega) = \sum_{l=0}^{\infty}\sum_{m=0}^{l}[A_{lm}^{(\alpha)}\cos m\phi + B_{lm}^{(\alpha)}\sin m\phi]\cdot P_l^m(\cos\theta)\,h_l^{(2)}(k_\alpha r) \tag{1.3}$$

where P_l^m is an associated Legendre function and $h_l^{(2)}$ a spherical Hankel function of the second kind. The multipolar coefficients $A_{lm}^{(\alpha)}$, $B_{lm}^{(\alpha)}$ are independent functions of frequency (Archambeau 1968) and contain information about the details of source geometry and prestress. The monopole term ($l = 0$) is used to represent the pressure pulse due to the explosion itself. If the failure zone retains spherical symmetry, and the prestress is pure shear, then the anomalous radiation is purely quadrupolar ($l = 2$). Let $R(t_0)$ be the failure zone radius,

function of the source time t_0, then the rupture velocity $V_R(t_0) = \dot{R}(t_0)$ may either be supersonic, trans-sonic or subsonic. For the sake of simplification and since the model is mostly appropriate for contained explosions, we shall assume henceforth that

$$\left.\begin{aligned} &V_s < V_p \leqslant V_R(t_0) && 0 \leqslant t_0 < \tau_p \\ &V_s \leqslant V_R(t_0) < V_p && \tau_p < t_0 \leqslant \tau_s \\ &V_R(t_0) < V_s < V_p && \tau_s < t_0 < \tau \\ &V_R(t_0) = 0 && \tau < t_0 \end{aligned}\right\}. \tag{1.4}$$

Let us define $\tau_i = \tau_s$, $i = 1, 2, 3$, and $\tau_4 = \tau_p$. Archambeau (1972) argued that if the rupture velocity is greater than the wave velocity in an interval $[0, \tau_\alpha]$ then the radiation field is identical to that which is due to the instantaneous creation, at time τ_α, of a cavity with radius $R(\tau_\alpha)$. Combining Archambeau's solutions for the subsonic and supersonic cases, we can write the multipolar coefficients in the form

$$\left\{\begin{aligned} &\begin{pmatrix} A_{lm}^{(\alpha)} \\ B_{lm}^{(\alpha)} \end{pmatrix} = \begin{pmatrix} a_{2m}'^{(\alpha)} \\ b_{2m}'^{(\alpha)} \end{pmatrix} k_\alpha^2 \tilde{V}_\alpha(\omega, \tau_\alpha) \\ &\tilde{V}_\alpha(\omega) = \frac{3}{V_\alpha} \int_0^\tau \exp(-i\omega t_0) R^2(t_0) \left[\dot{R}(t_0) H(t_0 - \tau_\alpha) + \frac{R(\tau_\alpha)}{3} \delta(t_0 - \tau_\alpha) \right] \cdot \frac{j_1(k_\alpha R(t_0))}{k_\alpha R(t_0)} dt_0 \end{aligned}\right. \tag{1.5}$$

where the 'static' coefficients $a_{2m}'^{(\alpha)}$, $b_{2m}'^{(\alpha)}$ depend on the elastic properties of the medium, as well as the prestress. Let us denote by $R_\alpha(t_0)$ the bracket appearing in the integrand.

Using the far-field approximation for the radial derivative of the spherical Hankel function

$$k_\alpha r \gg 1, \quad \frac{\partial}{\partial r} h_l^{(2)}(k_\alpha r) \simeq -\exp(-ik_\alpha r)/r, \tag{1.6}$$

we can summarize the results in the form

$$\left.\begin{aligned} &\tilde{\psi}_\alpha(\mathbf{r}, \omega) \simeq -C_\alpha(\theta, \phi) \frac{\exp(-ik_\alpha r)}{r} [\tilde{V}_\alpha(\omega)] \\ &C_\alpha(\theta, \phi) = \sum_{m=0}^{2} (a_{2m}'^{(\alpha)} \cos m\phi + b_{2m}'^{(\alpha)} \sin m\phi) P_2^m(\cos\theta) \end{aligned}\right\}. \tag{1.7}$$

The factor $C_\alpha(\theta, \phi)$ represents the radiation pattern, shown by Honda (1962) to be that of a double couple. $\tilde{V}_\alpha$ has been termed either the spectral variation (Ben Menahem 1962) or the reduced spectrum (Dahlen 1974). Without loss of generality we can assume that the pure shear prestress is in the (x, y) plane in such a way that only the component $\sigma_{13}^{(0)}$ is nonzero. In that case we have

$$\left.\begin{aligned} &b_{22}'^{(1)} = a_{20}'^{(2)}/6 = -a_{22}'^{(2)} = -b_{21}'^{(3)}/2 = \kappa_s \sigma_3^{(0)}/4 \\ &a_{21}'^{(4)} = \kappa_p \sigma_{13}^{(0)} \\ &\kappa_\alpha = \frac{5[1 - \sigma - \delta_{\alpha 4}\sigma]}{\mu(7 - 5\sigma)}, \quad 2\kappa_s/\kappa_p = (V_p/V_s)^2 \end{aligned}\right\} \tag{1.8}$$

and the other coefficients vanish (e.g. Minster 1973).

Combining (1.1), (1.5) and (1.7), we eventually get the double couple radiation found by Honda (1962) or Koyama (1973)

$$\left.\begin{aligned}
\tilde{u}_r(\mathbf{r},\omega) &= \kappa_p \frac{3\sigma_{13}^{(0)}}{2} \sin 2\theta \cos\phi \frac{\exp(-ik_p r)}{r} \tilde{V}_p(\omega) \\
\tilde{u}_\theta(\mathbf{r},\omega) &= \kappa_s 3\sigma_{13}^{(0)} \cos 2\theta \cos\phi \frac{\exp(-ik_s r)}{r} \tilde{V}_s(\omega) \\
\tilde{u}_\phi(\mathbf{r},\omega) &= -\kappa_s 3\sigma_{13}^{(0)} \cos\theta \sin\phi \frac{\exp(-ik_s r)}{r} \tilde{V}_s(\omega)
\end{aligned}\right\}. \tag{1.9}$$

It will be useful to cast the reduced spectrum in another form, and for this purpose we use the following result (Gradshteyn & Ryshik 1965)

$$2^\mu \Gamma(\mu+1)\, y^{-(\mu+1)} J_{\mu+1}(y) = \int_0^1 x(1-x^2)^\mu J_0(xy)\, dx \tag{1.10}$$

from which we deduce

$$j_1(k_\alpha R(t_0)) = \frac{k_\alpha}{R(t_0)} \int_0^{R(t_0)} \left(1 - \frac{\rho^2}{R^2(t_0)}\right)^{1/2} J_0(k_\alpha \rho)\, \rho\, d\rho$$

so that

$$\tilde{V}_\alpha(\omega) = \int_0^\tau dt_0 \exp(-i\omega t_0) \frac{3\dot{R}_\alpha(t_0)}{V_\alpha} \int_0^{R(t_0)} \left(1 - \frac{\rho^2}{R^2(t_0)}\right)^{1/2} J_0(k_\alpha \rho)\, \rho\, d\rho. \tag{1.11}$$

The spectral properties of (1.9) are well known, and we only need recall the major results:

(1) At high frequency, if the expansion includes a supersonic period, then $\tilde{V}_\alpha$ behaves as ω^{-2}. If the rupture velocity remains subsonic at all times, then $\tilde{V}_\alpha$ decays as ω^{-3} or faster.

(2) At low frequency, the spectrum is flat if the prestress field is pure shear in an infinite medium. The ratio of transverse components (*S*-wave) spectral amplitudes to radial component (*P*-wave) amplitudes is about $(V_s/V_p)^3$. One can define a seismic moment (Honda 1962; Aki & Tsai 1972; Randall 1973), equal to (for a Poisson solid)

$$M_0 = \frac{60}{23} \pi R^3(\tau)\, \sigma_{13}^{(0)}.$$

We shall see below that (1.11) is amenable to transformation into the time domain. But let us first discuss the solution in more detail.

2 Relaxation source and dislocation source

When cast in the form (1.9), (1.11), the stress relaxation solution bears a striking resemblance to that of a displacement dislocation. Such a resemblance for the instantaneous source has been pointed out by Snoke (1976) who uses it in order to compare corner frequencies and pulse durations for spherical and circular rupture models. The comparison can also be performed in the more general case considered here; in particular we shall show under which conditions the two geometries can be differentiated from the far-field pulses. The far-field

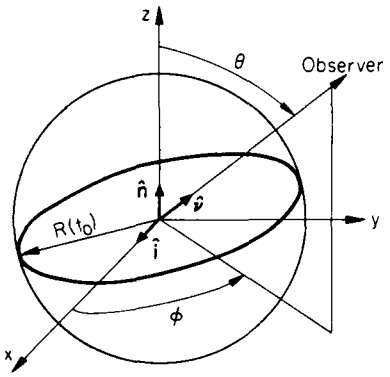

Figure 1. Geometry of spherical relaxation source and circular dislocation of same growth history.

displacement radiation spectrum in the direction $\tilde{\nu}$ due to a dislocation along the surface Σ of unit normal $\hat{n}$, with a Burgers vector $\mathbf{D}(\mathbf{r}_0, t_0)$ in the $\hat{\imath}$ direction (Fig. 1) is (e.g. Dahlen 1974)

$$\begin{cases} \mathbf{u}_p(\mathbf{r}, \omega) = \hat{v}\, \dfrac{2V_s^2}{4\pi V_p^3}\, \dfrac{\exp(-ik_p r)}{r}\, (\hat{v}\cdot\hat{n})\,(\hat{v}\cdot\hat{\imath})\, \tilde{W}_p(\omega) \\ \mathbf{u}_s(\mathbf{r}, \omega) = \dfrac{1}{4\pi V_s}\, \dfrac{\exp(-ik_s r)}{r}\, [2\hat{v}(\hat{n}\cdot\hat{v})\,(\hat{\imath}\cdot\hat{v}) - \hat{\imath}\,(\hat{n}\cdot\hat{v}) - \hat{n}\,(\hat{\imath}\cdot\hat{v})]\, \tilde{W}_s(\omega). \end{cases} \tag{2.1}$$

If Σ lies in the (x, y) plane and $\hat{\imath} = \hat{x}$, and if we choose spherical coordinates we get

$$\begin{cases} \tilde{u}_r(\mathbf{r}, \omega) = \dfrac{V_s^2}{4\pi V_p^3}\, \sin 2\theta \cos\phi\, \dfrac{\exp(-ik_p r)}{r}\, \tilde{W}_p(\omega) \\ \tilde{u}_\theta(\mathbf{r}, \omega) = \dfrac{1}{4\pi V_s}\, \cos 2\theta \cos\phi\, \dfrac{\exp(-ik_s r)}{r}\, \tilde{W}_s(\omega) \\ \tilde{u}_\phi(\mathbf{r}, \omega) = -\dfrac{1}{4\pi V_s}\, \cos\theta \cos\phi\, \dfrac{\exp(-ik_s r)}{r}\, \tilde{W}_s(\omega) \end{cases} \tag{2.2}$$

where the spectral variation is given by

$$\tilde{W}_\alpha(\omega) = \int_{-\infty}^{+\infty} \exp(-i\omega t_0)\, dt_0 \iint_{\Sigma(t_0)} i\omega D(\mathbf{r}_0, t_0) \exp(ik_s \mathbf{r}_0 \cdot \hat{v})\, d\mathbf{r}_0. \tag{2.3}$$

If $\Sigma(t_0)$ is the disk of radius $R(t_0)$ this becomes (e.g. Hoang 1974)

$$\tilde{W}_\alpha(\omega) = 2\pi \int_{-\infty}^{+\infty} \exp(-i\omega t_0)\, dt_0 \int_0^{R(t_0)} J_0(k_\alpha \rho \sin\theta)\, \dot{D}(\rho, t_0)\, \rho\, d\rho \tag{2.4}$$

where we assumed that the Burgers vector depends only on $\rho = (x_0^2 + y_0^2)^{1/2}$. This turns out to be a good assumption as witnessed by Madariaga's (1976) finite difference calculations of a growing circular shear crack.

The comparison of (1.11) and (2.4) shows immediately an important difference: whereas $\tilde{V}_\alpha$ does not depend on the angular variables, the argument of the Bessel function in (2.4) exhibits an explicit dependence of $\tilde{W}_\alpha$ on the observer's direction θ. It is easy to see that no distribution of $\mathbf{D}$ in the (x, y) plane will rid us of this problem. Molnar, Jacob & McCamy

(1973) and Dahlen (1974) explain that the presence of θ in (2.4) is due to interferences between radiation components originating from various points of Σ. The duration of the far field pulse – and the corner frequency – depend on θ.

Thus the double-couple radiation pattern in (2.2) does not represent the complete directional dependence of the field, which is frequency dependent. This can be stated formally by saying that the relaxation (spherical source) model is a separable source in the far-field, while the dislocation source is not separated. Another observation can be made immediately: it is clear that whenever a trans-sonic stage is involved – actually whenever $\tau_\rho \neq \tau_s$ – we shall need a different dislocation to match the *P*-wave radiation and the *S*-wave radiation, respectively. The reason is that, for a spherical failure zone with rupture velocity greater than the wave speed, the rupture front propagates faster than the wave front so that the medium cannot know of the failure phenomenon until $V_R(t_0)$ falls below the wave speed. On the contrary, radiation is emitted over the whole rupture duration for a planar dislocation whatever the rupture velocity. This does not mean that no dislocation can be found which would yield the same radiation field as (1.9). The only statement we can safely make is that we cannot find such a dislocation with Σ belonging to the (x, y) plane. Actually, we can extend this conclusion to any planar surface Σ since θ is present implicitly in (2.3). Thus any displacement dislocation equivalent to the separated solution (1.9) would have to be quite complicated.

On the other hand, comparison of (1.11) and (2.4) is quite instructive. It is clear that in the (x, y) plane, that is for $\theta = \pi/2$, we can proceed by identification and if the time τ_ρ is defined such that $R(\tau_\rho) = \rho$, we have

$$\dot{D}_\alpha(\rho, t_0) = 18\kappa_s \sigma_{13}^{(0)} \left(1 - \frac{\rho^2}{R^2(t_0)}\right)^{1/2} \dot{R}_\alpha(t_0)\, H(t_0 - \tau_\rho). \tag{2.5}$$

Using the definition of $\dot{R}_\alpha(t_0)$, this can be integrated to yield for $t_0 < \tau$

(1) $\tau_\rho < \tau_\alpha$

$$D_\alpha(\rho, t_0) = 18\kappa_s \sigma_{13}^{(0)} \left[(R^2(t_0) - \rho^2)^{1/2} - \tfrac{2}{3}(R^2(\tau_\alpha) - \rho^2)^{1/2} + \rho \arccos \frac{\rho}{R(\tau_\alpha)} - \rho \arccos \frac{\rho}{R(t_0)}\right] H(t_0 - \tau_\alpha) \tag{2.6a}$$

(2) $\tau_\alpha < \tau_\rho$

$$D_\alpha(\rho, t_0) = 18\kappa_s \sigma_{13}^{(0)} \left[(R^2(t_0) - \rho^2)^{1/2} - \rho \arccos \frac{\rho}{R(t_0)}\right] H(t_0 - \tau_\rho) \tag{2.6b}$$

and of course, for $\tau < t_0$, $D(\rho, t_0) = D(\rho, \tau)$.

It is remarkable that whenever there is no trans-sonic regime, i.e. the rupture velocity jumps from supersonic to subsonic, $\tau_p = \tau_s$ and the *P*- and *S*-dislocations are identical. Only where there is a trans-sonic interval are the dislocations different. It is easy to show, however, that

$$\int_0^{R(\tau)} D_\alpha(\rho, \tau)\, \rho\, d\rho$$

is the same for both so that the moment is the same for both.

In order to illustrate these functions, we choose a model which, although academic, is fairly general and includes the three regimes. We take $V_R(t_0) = 2V_s - t_0$, as described on Fig. 2. The displacement jumps $D_\alpha(\rho, t_0)$ are shown on Fig. 3 for several radii, and Fig. 4 depicts $D_\alpha(\rho, \tau)$, the final displacement, as a function of ρ (curves (b) and (c)).

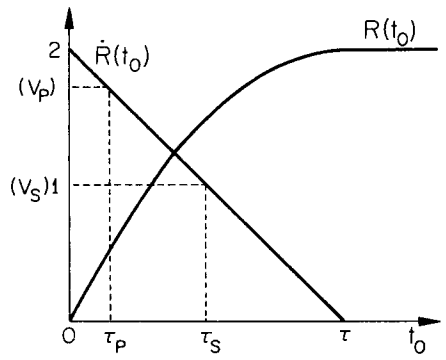

Figure 2. Rupture velocity and source radius as a function of time. Shear velocity is arbitrarily set to unity. Rupture velocity is successively supersonic, trans-sonic and subsonic.

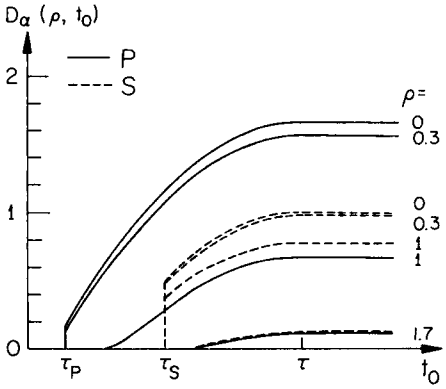

Figure 3. 'Equivalent' circular dislocation to a spherical relaxation source with growth history as in Fig. 2. Displacement jump is shown as a function of source time t_0 for selected radii ρ. Note the 'equivalent' dislocation is different for P and S radiation, for values of ρ such that rupture velocity is trans-sonic; for $\rho = 1.7, \dot{R} < V_S$ (Fig. 2) and the P and S waves become identical.

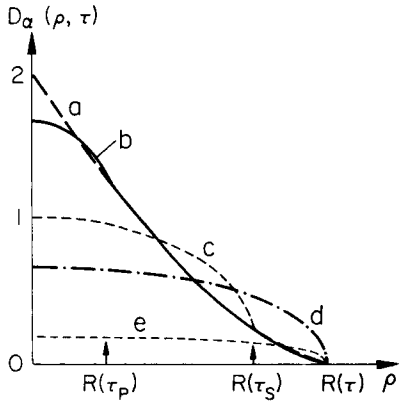

Figure 4. Final displacement jump as a function of radius: (b) and (c) correspond to P and S equivalent dislocations as described in Fig. 3, (a) P and S limiting curve if $\dot{R}(t_0)$ were subsonic for all t_0, (d) P and S curves if $\dot{R}(t_0)$ were supersonic for all t_0, (e) displacement jump for uniform stress release of $\sigma_{13}^{(0)}$ by circular shear crack.

In that case, a large fraction of the rupture duration corresponds to supersonic and transsonic regimes so that only for the outer ¼ of the final radius are the P and S dislocation functions identical. Notice how the P dislocation is much more concentrated towards the centre of the disk, while the S dislocation shows a broader distribution. The singular behaviour of the spherical relaxation source at times τ_p and τ_s, when the wave front and the rupture front coincide, is translated both in the displacement history and in the final displacement distribution.

Of interest is the case where $R(t_0) = V_R t_0$ with V_R a constant and $V_R < V_s$. Then we have the same equivalent dislocation for P and S, and

$$D(\rho, t_0) \propto \left[(V_R^2 t_0^2 - \rho^2)^{1/2} - \rho \arccos \frac{\rho}{V_R t_0}\right] H(t_0 - \tau_\rho) \tag{2.7}$$

(curve (a) on Fig. 4). This is different from the function found by Kostrov (1964) for the self similar circular shear fault, in the presence of the arccos term. From the investigation of Burridge & Willis (1969) and the comments of Dahlen (1974) we deduce that this difference implies a nonuniform stress drop for our dislocation. This can be understood quite easily if we think of the spherical geometry we started with: it is much more efficient at releasing stress near the z axis than away from it. The plots of (2.7) are very similar looking to the corresponding figures obtained numerically by Madariaga (1976) and we omit them. Another case of interest arises where $V_R(t_0)$ is supersonic at all times. The final displacement $D(\rho, \tau)$ is given by curve (d) on Fig. 4, and could be obtained from a circular shear crack, with a uniform stress release. The main results of the preceding discussion are summarized on Fig. 4, where the final static displacement jump $D(\rho, \tau)$ is plotted as a function of radius for a variety of cases. The first four curves are final static displacements of same total seismic moment, whereas curve (e) corresponds to the case of a uniform stress release of $\sigma_{13}^{(0)}$ by a circular shear crack (Keilis Borok 1959). The seismic moment is then only $M_0 = 16/7\ \sigma_{13}^{(0)} R^3(\tau)$. Thus, when using a spherical rupture, at constant seismic moment, we shall underestimate the stress release by a factor of $7 \times 60\pi/16 \times 23 \simeq 3.6$. This number is the geometrical factor to use when comparing stress release estimated from spherical rupture models with stress drop estimated from circular shear crack models. In other words curve (d) differs from curve (e) only in a factor of 3.6 in the stress release.

The argument which led to (2.5) is only strictly valid for $\theta = \pi/2$. At different azimuths, if we adopt this formula, (2.2) will not yield the fields defined by (1.9). There will be a residual field, difference between the dislocation and spherical source fields. This residual field will have the same double couple radiation pattern and a reduced spectrum given by (1.11), where $J_0(k_\alpha \rho)$ is replaced by $J_0(k_\alpha \rho \sin\theta) - J_0(k_\alpha \rho)$. It is clear that the maximum discrepancy occurs for $\theta = 0$, so that it can be bounded. We have

$$J_0(k_\alpha \rho \sin\theta) - J_0(k_\alpha \rho) = \frac{k_\alpha^2 \rho^2 \cos^2\theta}{4} - \frac{k_\alpha^4 \rho^4 (1 - \sin^4\theta)}{64} + \ldots \tag{2.8}$$

which is bounded by its first term, or $\pi^2 \lambda^{-2} \rho^2$, λ being the wavelength.

On intuitive grounds, this is is a satisfying result: the difference between the two models becomes important only for wavelengths of the order of, or smaller than the cavity radius. At high frequencies, where interference phenomena becomes significant, source geometry is more influential, and such effects are felt particularly in the direction perpendicular to the dislocation plane.

For the BILBY explosion (yield = 200 kT), Archambeau & Sammis (1970) find that the Rayleigh waves can be explained with a radius of ~ 400 m for the crushed zone, and prestress of ~ 70 bar. The period of the observations is about 20 s. Taking $V_p = 5$ km/s, we have

$\pi^2\lambda^{-2}\rho^2 \sim 1.6 \times 10^{-4}$. For Love waves with a period of 10 s this parameter is about 20^{-3}. In fact, for *SH* waves of period 1 Hz, the maximum discrepancy between the two radiation fields is measured by $\pi^2\lambda^{-2}\rho^2 \sim 0.2$, which is about the limit of precision for spectral amplitude measurements, considering the increasing importance of scattering by inhomogeneities, as well as increasing attenuation correction as one goes to higher and higher frequencies.

Thus the results of Snoke (1976) for instantaneous sources have been extended to the general case. The quantitative conclusion is that the radiation field generated by the spherical source can be adequately modelled with a dislocation source for wavelength down to about one third of the radius. Because of scattering and attenuation problems at high frequencies, one expects this limitation to play a role only for very large source dimensions. In addition, whenever the plane of the dislocation defined above is steeply dipping, far-field observations will correspond to $\theta \sim \pi/2$, so that in most cases, observations of the anomalous radiation field will indeed be adequately modelled by a dislocation equivalent source.

Similarities and differences between these two source models can be discussed in greater details from the far-field equivalent source functions.

3 Source functions

For the reduced spectra (1.11) or (2.5), the source function can be defined as

$$\begin{pmatrix} V_\alpha(t) \\ W_\alpha(t) \end{pmatrix} = \frac{1}{2\pi}\int_{-\infty}^{+\infty} \exp(i\omega t) \begin{pmatrix} \tilde{V}_\alpha(\omega) \\ \tilde{W}_\alpha(\omega) \end{pmatrix} d\omega. \tag{3.1}$$

Let us compute $W_\alpha(t)$, $V_\alpha(t)$ is then obtained from this result by taking $\theta = \pi/2$.

We have from (1.10), (1.4) and (2.5)

$$W_\alpha(t) = 18\kappa_s \sigma_{13}^{(0)} \sqrt{(\pi/2)} \int_{-\infty}^{+\infty} d\omega \int_0^\tau \exp[i\omega(t-t_0)]\, R^{1/2}(t_0)\, \dot{R}_\alpha(t_0)\, (k_\alpha \sin\theta)^{-3/2}$$
$$\times J_{3/2}(k_\alpha \sin\theta\, R(t_0))\, dt_0. \tag{3.2}$$

We can switch the order of integration and, on account of the evenness of $x^{-3/2}J_{3/2}(x)$, use the following result (Erdelyi *et al.* 1954)

$$\int_0^\infty x^{-\nu} J_\nu(ax) \cos xy\, dx = \sqrt{\pi}\, (2a)^{-\nu}\, \Gamma^{-1}(\nu + 1/2)\, (a^2 - y^2)^{\nu - 1/2}\, H(a^2 - y^2) \tag{3.3}$$

so that

$$\begin{cases} W_\alpha(t) = 9\kappa_s \sigma_{13}^{(0)}\, \pi\, \dfrac{V_\alpha^3}{\sin^3\theta}\, I_\alpha(t) \\ I_\alpha(t) = \displaystyle\int_0^\tau \frac{\dot{R}_\alpha(t_0)}{R(t_0)} \left[\left(\frac{R(t_0)\sin\theta}{V_\alpha}\right)^2 - (t-t_0)^2\right] H\left[\left(\frac{R(t_0)\sin\theta}{V_\alpha}\right)^2 - (t-t_0)^2\right] dt_0. \end{cases} \tag{3.4}$$

In order to evaluate $I_\alpha(t)$, we first have to discuss its limits. In the general case, the interval of integration may have to be broken into several intervals, intersections of $[\tau_\alpha, \tau]$ and the intervals in which the argument of the Heaviside distribution in (3.4) is positive. The integral may be evaluated numerically for any function $R(t_0)$ given numerically (e.g. results of a numerical shock calculation), but it can also be evaluated analytically for a wide variety of functions $R(t_0)$. This is true in particular whenever $R(t_0)$ admits a piecewise polynomial representation. In this paper, we shall assume that the rupture velocity $V_R(t_0)$ is a piecewise

linear function of t_0, so that $R(t_0)$ is piecewise parabolic. This includes the case of piecewise constant rupture velocity. It is clear that, to the accuracy of seismic measurements, most situations can be adequately modelled in this fashion.

Following Archambeau (1972) we take the rupture velocity to be supersonic prior to $t_0 = \tau_p$, and assume that $R(\tau_p)$ is known, so that the details of rupture propagation prior to τ_p do not directly concern us. For $0 \leqslant \tau_p \leqslant t_0 \leqslant \tau$, we choose a representation in the form

$$\begin{cases} \dot{R}(t_0) = V_R(t_0) = A(t_0 - \tau_p) + V_R(\tau_p) \\ R(t_0) = \dfrac{A}{2}(t_0 - \tau_p)^2 + V_R(\tau_p)(t_0 - \tau_p) + R(\tau_p). \end{cases} \tag{3.6}$$

For simplicity we suppose that the 'acceleration' A is non positive. $V_R(\tau_p)$ may be transsonic or subsonic. Let R_0 be the final radius, so that the rupture duration τ is solution of $R(\tau) = R_0$. The main cases which we shall take into consideration are

(1) $\dot{R}(t_0) = V_R(t_0) = V_R$ constant

(2) $\dot{R}(t_0) = V_R(t_0) = V_R(\tau_p)\left(1 - \dfrac{t_0 - \tau_p}{\tau - \tau_p}\right)$

In the second case, the rupture velocity decreases linearly from $V_R(\tau_p)$ to $V_R(\tau) = 0$. It is easy to see that the average rupture velocity in that case is $V_R(\tau_p)/2$, and is therefore subsonic. From (3.6), it is seen that the assumption of constant V_R is tantamount to taking $A = 0$.

We write

$$\begin{cases} R(t_0) = \dfrac{A}{2}(t_0 - z_1)(t_0 - z_2) \\ z_{(\frac{1}{2})} = [-V_R(\tau_p) \pm \sqrt{(V_R^2(\tau_p) - 2AR(\tau_p))}]/A + \tau_p. \end{cases} \tag{3.7}$$

The integral $I_\alpha(t)$ is evaluated in Appendix A in terms of the quantities z_1, z_2 and T_i, T_f, the limits of integration of $I_\alpha(t)$ which themselves depend on the wave type, and are shown in Appendix B. $I_\alpha(t)$ is also given in the appendix for the cases of subsonic and supersonic constant rupture velocity for $0 \leqslant t_0 \leqslant \tau$. Except for the double-couple radiation pattern effect, we get for the displacement far-field pulses

$$\begin{pmatrix} u_r(t) \\ u_\theta(t) \\ u_\phi(t) \end{pmatrix} = {}^9\!/_4 \kappa_s \sigma_{13}^{(0)} V_s^2 (\sin\theta)^{-3} \begin{pmatrix} I_p(t) \\ I_s(t) \\ I_s(t) \end{pmatrix}. \tag{3.8}$$

It would seem from (3.8) that difficulties arise in the vicinity of $\theta = 0$. But $I_\alpha(t)$ depends on θ too, both explicitly and through T_i and T_f and it can be shown that the case $\theta = 0$ is obtained by letting θ approach 0 continuously. In fact, when V_R is constant and subsonic for $0 \leqslant t_0 \leqslant \tau$, we have from the results given in Appendix A

$$I_\alpha(t) = {}^4\!/_3 \xi_\alpha^3 \sin^3\theta + 0(\sin\theta^5), \quad \theta \ll 1, \quad \xi_\alpha = V_R/V_\alpha.$$

If V_R is supersonic, and $\theta \ll 1$

$$I_\alpha(t) \sim [\xi_\alpha^2 \theta^2 \tau^2 - (t - \tau)^2]\, H[\xi_\alpha^2 \theta^2 \tau^2 - (t - \tau)^2]$$

From (3.8) the pulse is an arc of parabola of width proportional to θ and maximum amplitude inversely proportional to θ: it is a Dirac distribution for $\theta = 0$. This is confirmed by the calculation of the area under the pulse, which is $4R_0^3/V_\alpha^3$, independent of θ. It may be shown that the area under the pulse is independent of θ in the general case, in agreement with the result of Savage (1966), but the algebra is quite tedious and we omit it.

4 Examples of far-field waveforms

In order to illustrate the foregoing discussion, we have evaluated (3.8) in a wide variety of cases and present below examples of such calculations. In all cases the fields generated by the dislocation source introduced in Section 2 have been computed, the waveforms originating from the spherical relaxation source are then simply obtained by choosing $\theta = \pi/2$. All waveforms are computed as a function of the reduced time $t - r/V_\alpha$ ($V_\alpha = V_p$ or V_s).

Fig. 5 shows a sequence of waveform pairs corresponding each to a different, constant subsonic rupture velocity. The amplitude scale is arbitrary since only the wave shape is of interest to us. From Appendix A, in each case the signal ends at $t - r/V_\alpha = R_0/V_R + R_0/V_\alpha$.

It is immediately clear that the dominant effect shaping the waveform is that of the 'stopping phase'. Indeed, as the rupture velocity decreases, whereas the waveforms become more and more emergent, and the parabolic portions longer and longer, the decay time undergoes little variation. This is to be expected since the abrupt termination of the rupture process is clearly the most prominent feature of this model.

One interesting, if puzzling, feature is that the P waveform is in all cases more emergent than the S waveform. This is due to a combination of both the pulse shape and the relative amplitude of P and S pulses. It is readily evident that the cause of this stems from the inequality $V_R/V_p < V_R/V_s$. On the other hand, such signals are usually observed through band pass instruments, so that the emergent beginning of the signal may be lost in the background noise. One might therefore expect that P arrival times be read systematically late with respect to the S arrival time (Suteau 1975). Let us emphasize here that the effect suggested here is purely a source effect, independent of wave propagation and attenuation mechanisms. The interesting aspect of this observation is that this effect is tantalizingly reminiscent of the 'z-phenomenon' (e.g. Jeffreys 1927, 1937; Benioff 1938; Gutenberg & Richter 1943), as suggested by Minster (1973) and Suteau (1975). That is, the apparent

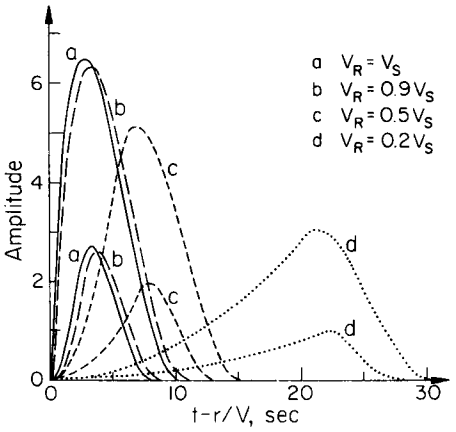

Figure 5. Pairs of far field waveforms for $\theta = \pi/2$ (i.e. spherical relaxation source), and constant, subsonic rupture velocity. $V_p = 8.67$ km/s, $V_s = 5$ km/s, $R_0 = 25$ km. Amplitudes are arbitrary, but true S to P relative amplitudes are represented.

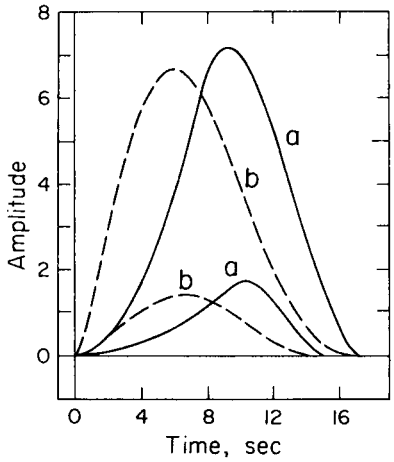

Figure 6. Same parameters as in Fig. 5, $\theta = \pi/2$. (a) V_R is constant 2 km/s, (b) V_R decreases linearly from 4 km/s at $t_0 = 0$ to 0 at $t_0 = \tau$.

origin time of *S* waves should be anterior to that of *P* waves. What is suggested here is that the apparent origin time of both *P* and *S* waves might be late with respect to the true origin time, but less so for *S* waves than for *P* waves. On the other hand this is merely a suggestion since (1) this is a visual bias, the magnitude of which is strongly affected by actual amplitudes, and (2) wave propagation and attenuation could introduce effects of the same magnitude or larger (e.g. Liu, Anderson & Kanamori 1976). Further, since the *S* wave is usually preceded by other arrivals, *S* times measurements may be biased due to a number of other causes. In addition, source functions required to explain simultaneously long-period and short-period observations (e.g. Burdick & Mellman 1976) are certainly more akin to pulse (a) than to pulse (d), suggesting that the rupture velocity may be larger, at least during the first stages of the phenomenon. Such a possibility is illustrated on Fig. 6, where both sets of waveforms correspond to the same average value of V_R. But, whereas V_R is constant for waveforms (a), it decreases linearly for waveforms (b). It is clear that the onset of the source function is much sharper in the case (b), and could be rendered even sharper with a more complicated rupture velocity history.

The modification of the waveforms as a function of θ is illustrated on Fig. 7. These results parallel those of Savage (1966) or Madariaga (1976). The main effect of the circular

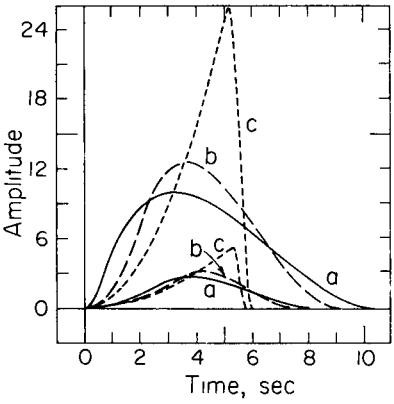

Figure 7. Same parameters as in Fig. 5, $V_R = 4.5$ km/s $= 0.9\,V_S$. (a) $\theta = \pi/2$, (b) $\theta = \pi/4$, (c) $\theta \simeq 0$ (5° for computational purposes).

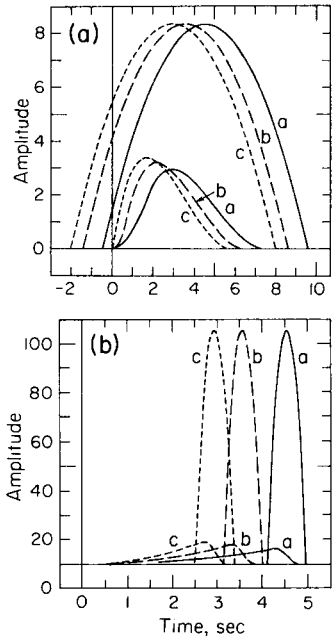

Figure 8. (a) Same parameters as in Fig. 5. $\theta = \pi/2$, case of trans-sonic rupture velocity. (a) V_R = 5.5 km/s, (b) V_R = 7.0 km/s, (c) V_R = 8.5 km/s. (b) Same as Fig. 8(a). $\theta \simeq 0$ (5° for computational purposes).

dislocation geometry is a relative enhancement of the stopping phase as θ decreases. The areas under the curves are the same for sets (a), (b) and (c), as they should be since the seismic moment is the same for the three cases.

Fig. 8 shows how waveforms are affected when the rupture velocity is allowed to be trans-sonic. Fig. 8(a) corresponds to $\theta = \pi/2$ and Fig. 8(b) to $\theta \simeq 0$ (5° for computational purposes). As shown earlier, in that case, one must introduce different dislocation sources to model the P pulse and the S pulse generated by a spherical relaxation source. The results depicted in Fig. 8 are in agreement with Snoke's (1976) observation that rupture velocities greater than the wave velocity will cause the waveform to become an arc of parabola, centred at $t = R_0/V_R$, and of width $2V_R \sin\theta/V_\alpha$. For supersonic rupture velocities, the P pulse would also become an arc of parabola, and as $V_R \to \infty$, both P and S pulse tend to arcs of parabola centred at the origin, which is the case calculated by Snoke.

An interesting aspect of Fig. 8(a) is that the S onset time is earlier than the P onset time. This is due to the fact that the source (spherical relaxation model) grows faster than the S signal is propagated, so that the S first arrival is radiated by the source point closest to the observer, rather than by the point of initial rupture. This is precisely analogous to the mechanism proposed by Reid (1918) and Benioff (1938) in order to explain the 'z-phenomenon'. Such a mechanism is purely geometrical as opposed to the comment made earlier concerning Fig. 5. On the other hand the onset times of Fig. 8(b) are controlled by our definition of the 'equivalent' dislocation, whereby different circular dislocations are used to model P and S pulses. In particular, the dislocation used for the S pulse is created instantaneously at $t = \tau_s = \tau$ in this case, and the arc of parabola tends to a Dirac distribution at $t - r/V_s = \tau$ as $\theta \to 0$. For $\theta \to 0°$ and $V_R \to \infty$ both P and S pulses would become Dirac pulses at the origin.

The results obtained in this paper allow us to assess the effect of the 'transparency' assumption on the far-field waveforms. Fig. 9(a) and (b) compare our solution with two

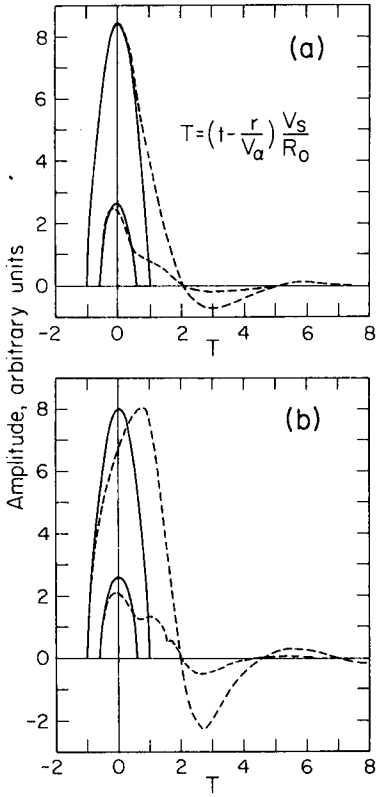

Figure 9. Comparison of pulses using 'transparent' source approximation, with exact solutions (dashed lines) presented by Koyama *et al.* (1973) for the instantaneous case ($\theta = \pi/2$). (a) Cavity model. (b) Liquefaction model.

solutions presented by Koyama *et al.* (1973). In both cases a failure zone of radius R_0 is created instantaneously; Fig. 9(a) corresponds to the case of a spherical cavity, Fig. 9(b) to the case where the material inside the failure zone is liquefied, the acoustic velocity inside the liquid being equal to the shear velocity outside the failure zone. The waveforms have been normalized so as to equalize the amplitude of the S wave, and are plotted as a function of a dimensionless reduced time. It is clear that the 'transparent' solution developed in this paper is a much better approximation in the cavity case than in the liquefaction case. This is presumably due to the inertial effects generated by the presence of liquid inside the failure zone, which are obviously ignored in the 'transparent' solution. In both cases, one observes that the 'transparent' waveform is aborted and has a sharp termination. This is due to two effects: (1) Because of transparency, radiation generated by the 'far' side of the failure zone is allowed to propagate through the sphere as if it were absent; in particular the 'stopping phase' generated by the far side arrives too early. (2) Oscillations of the failure zone are ignored, by the very definition of 'transparency', so that the oscillating tail of the waveform cannot be obtained from our solution.

A similar comparison is shown on Fig. 10. In that case a spherical cavity grows with a constant rupture velocity of $0.5\,V_s$. The waveforms shown in dashed lines are Burridge's (1975) solutions. Once more our solution exhibits an early stopping phase, and lacks the oscillating behaviour after the main pulse. The interpretation is the same as above. Note, however, that in all three Figs 9–10, the beginning of the pulse is modelled very well by the

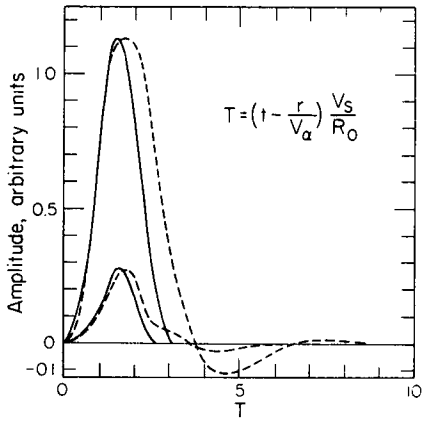

Figure 10. Comparison of waveforms with Burridge's (1975) solution (dashed lines). $V_R = 0.5\,V_s$, $\theta = \pi/2$.

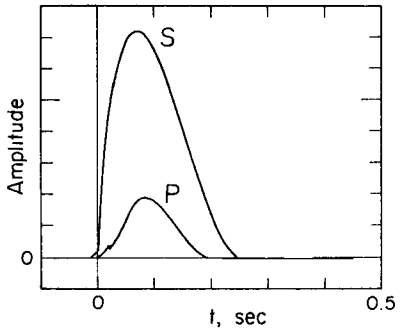

Figure 11. Far-field tectonic release pulses for BILBY underground explosion model of Archambeau & Sammis (1970). $V_p = 5.5$ km/s, $V_s = 3.2$ km/s, $V_R = 6$ km/s for $0 \leqslant R \leqslant 75$ m, $V_R = 3$ km/s for $75 \leqslant R \leqslant 420$ m.

transparent source, and that the general pulse shape is quite adequate for seismological purposes.

One last example of waveform calculation is shown on Fig. 11. These are the far-field waveforms corresponding to the tectonic release model proposed by Archambeau & Sammis (1970) for the BILBY event. The cavity radius is assumed to grow supersonically to a value of 75 m, and then subsonically ($V_R \sim 0.9\,V_s$) to a final value of 400 m. It is immediately clear that the very brief, supersonic stage has hardly any noticeable effect on the waveforms (small 'kinks') and should be quite difficult to investigate, especially after propagation of such pulses through an attenuating earth model. In other words, the only parameter which appears to have a significant effect on the waveform is the final cavity size, which Archambeau & Sammis identify with the zone of intense fracturing and weakening of the material around the shot point. This is basically in agreement with the conclusion of the authors, obtained on the basis of long-period surface-wave observations. In order to discuss their estimate of the prestress $\sigma_{13}^{(0)}$ we would have to calculate the amplitude of the pulse (3.8) after propagation through an earth model and an instrument, and adjust $\sigma_{13}^{(0)}$ so as to match observations. Such an exercise is outside the scope of the present paper.

Conclusions

We have used the far-field approximation to calculate theoretical seismic pulses ('source function') generated by a spherical cavity growing in an initial shear field. The transparent

source approximation leads to a significant simplification of the problem. It has been shown how a circular dislocation source model which yields identical far-field pulses – except for directivity effects – provided that the rupture velocity is either subsonic or supersonic. For trans-sonic rupture velocities, two different dislocation models must be introduced in order to model separately the P and S pulses. Source geometry has a significant effect on the radiation field only for wavelengths smaller than about one third of the source radius. Because higher frequency waveforms are easily degraded in the Earth due to attenuation and scattering effects, we conclude that, except for very large sources, the anomalous radiation from underground explosions can in most cases be modelled quite adequately in the far-field by a dislocation source model, whether faulting actually occurs or not.

The far-field pulses can be obtained in analytical form if the cavity radius is given as a function of time. We have complemented the analytical results with a few calculations which illustrate the dependence of waveforms on the various source parameters, in particular the growth history of the source. Comparisons with exact solutions in three simple cases show that the main effects of the transparency approximation are (1) a pulse of somewhat shorter duration, and (2) elimination of some details in the pulse shape due to oscillations of the source region.

Because of the simplicity of the general results, even in the case of fairly complicated source history, the solutions presented here are readily adaptable for use as input to a generalized ray theory program (e.g. Helmberger 1974), or for that matter, to any wave propagation program.

Acknowledgments

Part of this research was completed as both authors were at the Institut de Physique du Globe de Paris, and was supported by Institut National d'Astronomie et de Geophysique.

We are grateful to Dr C. B. Archambeau and an anonymous reviewer for useful criticisms and suggestions.

Calculations were performed at the Seismological Laboratory of the California Institute of Technology. This research was partly supported by the Advanced Research Projects Agency of the Department of Defense and was monitored by the Air Force Office of Scientific Research under Contract No. F44620-72-C-0078.

References

Aki, K., 1964. A note on surface wave generation from the Hardhat nuclear explosion, *J. geophys. Res.*, **69**, 1131.

Aki, K., Reasenberg, P., DeFazio, T. & Tsai, Y. B., 1969. Near-field and far-field seismic evidence for triggering of an earthquake by the Benham explosion, *Bull. seism. Soc. Am.*, **59**, 2197.

Aki, K. & Tsai, Y. B., 1972. Mechanism of Love-wave excitation by explosive sources, *J. geophys. Res.*, **77**, 1452.

Archambeau, C. B., 1964. Elastodynamic source theory, *PhD thesis, California Institute of Technology*, Pasadena.

Archambeau, C. B., 1968. General theory of elastodynamic source fields, *Rev. Geophys.*, **16**, 241.

Archambeau, C. B., 1972. The theory of stress wave radiation from explosions in prestressed media, *Geophys. J. R. astr. Soc.*, **29**, 329.

Archambeau, C. B. & Sammis, C., 1970. Seismic radiation from explosions in prestressed media and the measurement of tectonic stress in the earth, *Rev. Geophys.*, **8**, 473.

Benioff, H., 1938. The determination of the extent of faulting with application to the Long Beach earthquake, *Bull. seism. Soc. Am.*, **28**, 77.

Ben Menahem, A., 1962. Radiation of seismic body waves from a finite moving source, *J. geophys. Res.*, **67**, 345.

Brune, J. N. & Pomeroy, P. W., 1963. Surface wave radiation patterns for underground nuclear explosions and small magnitude earthquakes, *J. geophys. Res.*, **68**, 5005.

Burdick, L. & Mellman, G., 1976. Inversion of the body waves from the Borrego Mountain earthquake to the source mechanism, *Bull. seism. Soc. Am.*, **66**, in press.

Burridge, R., 1975. The pulse shapes and spectra of elastic waves generated when a cavity expands in an initial shear field, *J. geophys. Res.*, **80**, 2606.

Burridge, R. & Willis, J. R., 1969. The self-similar problem of the expanding elliptical crack in an anisotropic solid, *Proc. camb. Phil. Soc.*, **66**, 443.

Dahlen, F. A., 1974. On the ratio of *P*-wave to *S*-wave corner frequencies for shallow earthquake sources, *Bull. seism. Soc. Am.*, **64**, 1159.

Erdelyi, A., Magnus, Oberhettinger, F. & Tricomi, F. G., 1954. *Tables of integral transforms*, Vol. 1–2, Bateman Manuscript Project, California Institute of Technology, McGraw-Hill Book Company, New York.

Gradshteyn, I. S. & Ryshik, I. M., 1965. *Table of integrals, series, and products*, Academic Press, New York, and London.

Gutenberg, B. & Richter, C. F., 1943. Apparent origin times of $\bar{S}$, *Bull. seism. Soc. Am.*, **33**, 269.

Harkrider, D. G., 1976. Theoretical potentials and displacements for two seismic sources, *Geophys. J. R. astr. Soc.*, **47**, 97.

Helmberger, D. V., 1974. Generalized ray theory for shear dislocations, *Bull. seism. Soc. Am.*, **64**, 45–64.

Hirasawa, T. & Sato, R., 1963. Propagation of elastic waves from a spherical origin, *Zisin*, **916**, 52.

Hoang, T. P., 1974. Caracterisation des Sources Sismiques au Moyen des Spectres de l'Onde P. Application a l'Etude de quelques Seismes de l'Hindou-Kouch, *These de Doctorat d'Etat*, Strasbourg.

Honda, H., 1962. Earthquake mechanism and seismic waves, *J. Phys. Earth*, **10**, 2.

Jeffreys, H., 1927. On two British earthquakes, *Mon. Not. R. astr. Soc. Geophys. Suppl.*, **1**, 483.

Jeffreys, H., 1937. A further study of near earthquakes, *Mon. Not. R. astr. Soc. Geophys. Suppl.*, **4**, 196.

Keilis-Borok, V. I., 1959. On estimation of the displacement in an earthquake source, and of source dimensions, *Ann. Geofis.*, **12**, 205.

Kostrov, B. V., 1964. Self-similar problems of propagation of shear cracks, *J. appl. Math. Mech. (PMM)*, **28**, 1077.

Koyama, J., Horiuchi, S. E. & Hirasawa, T., 1973. Elastic waves generated from sudden vanishing of rigidity in a spherical region, *J. Phys. Earth*, **21**, 213.

Lambert, D. G., Flinn, E. A. & Archambeau, C. B., 1972. A comparative study of the elastic wave radiation from earthquakes and underground explosions, *Geophys. J. R. astr. Soc.*, **29**, 403.

Liu, H. P., Anderson, D. L. & Kanamori, H., 1976. Velocity dispersion due to anelasticity; implications for seismology and mantle composition, *Geophys. J. R. astr. Soc.*, **47**, 41.

Madariaga, R., 1976. Dynamics of an expanding circular fault, *Bull. seism. Soc. Am.*, **66**, 639.

Minster, J. B., 1973. Elastodynamics of failure in a continuum, *PhD thesis, California Institute of Technology*, Pasadena.

Molnar, P., Jacob, K. H. & McCamy, K., 1973. Implications of Archambeau's earthquake source theory of slip on faults, *Bull. seism. Soc. Am.*, **63**, 101.

Randall, M. J., 1964. On the mechanism of earthquakes, *Bull. seism. Soc. Am.*, **54**, 1283.

Randall, M. J., 1973. Low frequency spectra in seismic waves from explosions, *Geophys. J. R. astr. Soc.*, **32**, 387.

Reid, H. F., 1918. The starting points of earthquake vibrations, *Bull. seism. Soc. Am.*, **8**, 79.

Savage, J. C., 1966. Radiation from a realistic model of faulting, *Bull. seism. Soc. Am.*, **56**, 577.

Snoke, J. A., 1976. Archambeau's elastodynamical source-model solution and low-frequency spectral peaks in the far-field displacement amplitude, *Geophys. J. R. astr. Soc.*, **44**, 27.

Suteau, A. M., 1975. Dispersion differentielle des Ondes de Volume due au Processus de Rupture a la Source, *These de Doctorat de 3eme cycle;* Universite de Paris VI.

Contribution No. 219, Institut de Physique du Globe de Paris.
Contribution No. 2806, Division of Geological and Planetary Sciences, California Institute of Technology, Pasadena, California 91125.

Appendix A: calculation of the waveform

We have to evaluate the integral

$$I_\alpha(t) = \int_{T_i}^{T_f} \frac{\dot{R}_\alpha(t_0)}{R(t_0)} \left(\frac{\dot{R}^2(t_0) \sin^2\theta}{V_\alpha^2} - (t - t_0)^2 \right) dt_0 \qquad \text{(A1)}$$

where

$$\tau_\alpha \leqslant T_i < T_f \leqslant \tau$$

$$\dot{R}_\alpha(t_0) = \dot{R}(t_0)\, H(t_0 - \tau_\alpha) + \frac{R(\tau_\alpha)}{3}\, \delta(t_0 - \tau_\alpha).$$

$$R(t_0) = A/2\,(t_0 - z_1)\,(t_0 - z_2), \quad z_2 \leqslant T_i < T_f \leqslant z_1.$$

The first term in the integrand does not raise any difficulty. The only algebra required is the calculation of

$$J_\alpha(t) = \int_{T_i}^{T_f} (t_0 - t)^2\, \frac{-2t_0 - (z_1 + z_2)}{(t_0 - z_2)\,(z_1 - t_0)}\, dt_0. \tag{A2}$$

Integration by parts yields

$$J_\alpha(t) = \left[(t_0 - t)^2 \ln (t_0 - z_2)\,(z_1 - t_0)\right]_{T_i}^{T_f} - 2\int_{T_i}^{T_f} (t_0 - t) \ln (t_0 - z_2)\,(z_1 - t_0)\, dt_0. \tag{A3}$$

But we have, for instance

$$\int_{T_i}^{T_f} 2\,(t_0 - t) \ln (t_0 - z_2)\, dt_0 = \left[(t_0 - z_2)^2 \ln (t_0 - z_2) - \frac{(t_0 - z_2)^2}{2}\right]_{T_i}^{T_f}$$

$$- 2\,(t - z_2)\left[(t_0 - z_2) \ln (t_0 - z_2) - (t_0 - z_2)\right]_{T_i}^{T_f}.$$

Evaluating the corresponding integral for z_1, and reducing the result, one gets

$$J_\alpha(t) = (T_f - T_i)\,(T_f + T_i + z_1 + z_2 - 4t) + (z_1 - t)^2 \ln \frac{T_f - z_1}{T_i - z_1} + (z_2 - t)^2 \ln \frac{T_f - z_2}{T_i - z_2} \tag{A4}$$

so that

$$I_\alpha(t) = \frac{1}{3}\left[\frac{\sin^2\theta}{V_\alpha^2}\, R^2(\tau_\alpha) - (t - \tau_\alpha)^2\right] \delta(\tau_\alpha - T_i) + \frac{\sin^2\theta}{2V_\alpha^2}\, [R^2(T_f) - R^2(T_i)] - J_\alpha(t). \tag{A5}$$

Note that one may have $T_i = z_1 = T_f = 0$ when $\tau = 0$ and $t = 0$ but that this does not pose a real problem since it is easy to verify the continuity of $J_\alpha(t)$. Note also that (A5) is in a form suitable for computer programming. If $R(t_0)$ is of the form $V_R t_0$ where $V_R < V_\alpha$, these expressions can be greatly simplified, since there is no supersonic nor trans-sonic regime. One gets from (A1), or with more difficulty, from (A5):

$$I_\alpha(t) = (\xi_\alpha^2 \sin^2\theta - 1)\, \frac{T_f^2 - T_i^2}{2} + 2t\,(T_f - T_i) - t^2 \ln \frac{T_f}{T_i} \tag{A6}$$

where now $\xi_\alpha = V_R/V_\alpha$ and

$$T_i = \frac{t}{1 + \xi_\alpha \sin\theta}; \quad T_f = \frac{t}{1 - \xi_\alpha \sin\theta} \quad \text{for} \quad 0 < t < \tau(1 - \xi_\alpha \sin\theta)$$

$$T_i = \frac{t}{1 + \xi_\alpha \sin\theta}; \quad T_f = \tau = \frac{R_0}{V_R} \quad \text{for} \quad \tau(1 - \xi_\alpha \sin\theta) < t < \tau(1 + \xi_\alpha \sin\theta).$$

From these formulae, it is immediately clear that the pulse has a parabolic beginning, for

$0 < t < \tau(1 - \xi_\alpha \sin\theta)$, except in the case of a sonic rupture velocity.

If $V_R > V_\alpha$, then

$$I_\alpha(t) = (\xi_\alpha^2 \sin^2\theta\, \tau^2 - (t-\tau)^2)\, H\,[\xi^2 \sin^2\theta\, \tau^2 - (t-\tau)^2] \tag{A7}$$

which is in agreement with the result of Snoke (1976), for $V_R \to \infty$ with $V_R \tau$ finite.

Appendix B: limits of the integral $I_\alpha(t)$

The limits of the integral $I_\alpha(t)$ defined in (3.4) are determined by

$$\left.\begin{aligned} &R^2(t_0)\frac{\sin^2\theta}{V_\alpha^2} \geqslant (t-t_0)^2 \\ &\tau_\alpha \leqslant t_0 \leqslant \tau \end{aligned}\right\} \tag{B1}$$

where $R(t_0)$ is given by (3.7) so that

$$R(t_0) = A/2\,(t_0 - z_1)\,(t_0 - z_2). \tag{B2}$$

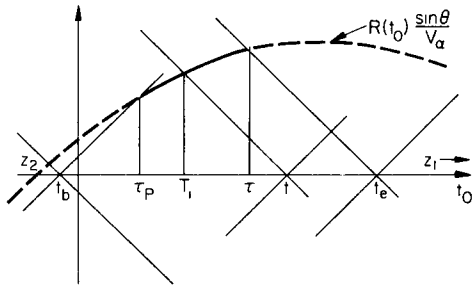

Figure 12. Graphical evaluation of integration limits in Appendix B.

The best way to investigate (B1) is graphically. Consider on Fig. 12 the parabola representing $R(t_0)\sin\theta/V_\alpha$ and more specifically the arc of it such that $\tau_\alpha \leqslant t_0 \leqslant \tau$. Then the interval of integration for a given time t is the interval such that this arc lies above both lines of equations $y = t_0 - t$ and $y = t - t_0$.

It is clear that the signal begins at

$$t_b = \tau_p - R(\tau_p)\frac{\sin\theta}{V_\alpha}$$

and ends at

$$t_e = \tau + R(\tau)\frac{\sin\theta}{V_\alpha}.$$

For intermediate times the interval of integration varies with t. The case shown on the figure would yield the integration limits T_i and τ.